Cisplatin Binding to DNA Oligomers from Hybrid Car-Parrinello/Molecular Dynamics Simulations

Katrin Spiegel,[†,‡] Ursula Rothlisberger,[§] and Paolo Carloni*[,†,‡]

SISSA, International School for Advanced Studies, 34100 Trieste, Italy, DEMOCRITOS, Modeling center for research in atomistic simulation, INFM, Italy, and EPFL, Ecole polytechnique fédérale de Lausanne, Institute of Molecular and Biological Chemistry, 1015 Ecublens, CH

Received: July 30, 2003; In Final Form: November 26, 2003

The structure and binding of cisplatin to DNA in aqueous solution are investigated via a QM/MM methodology. In our approach, the platinated moiety is treated at the density functional level and the biomolecular frame with the AMBER force field. The calculations are based on X-ray structures of platinated DNA in the free form (cispt-d(CCTCTG*G*TCTCC)-d(GGAGACCAGAGG) [Takahara, et al. *Nature* **1995**, *377*, 649−652][1]) and in complex with HMG protein domain A (cispt-d(CCUCTCTG*G*ACCTTCC)-d(GGAGAGACCTG-GAAGG) [Ohndorf et al. *Nature* **1999**, *399*, 708−712][2] as well as on a cisplatin docked DNA model. During the QM/MM simulation, the structure of the platinated DNA dodecamer rearranges significantly toward structural determinants of the solution structure as obtained by NMR spectroscopy [Gelasco et al. *Biochemistry* **1998**, *37*, 9230−9239].[3] The calculated ^{195}Pt chemical shifts of the QM/MM structure relative to cisplatin in aqueous solution are in qualitative agreement with the experimental data [Bancroft et al. *J. Am. Chem. Soc.* **1990**, *112*, 6860−6871. Miller et al. *Inorg. Chem.* **1985**, *24*, 2421−2425].[4,5] The QM/MM structure of the platinated/DNA HMG complex, on the other hand, remains rather similar to the X-ray structure, consistent with its relatively low flexibility. Docking of $Pt(NH_3)_2^{2+}$ onto DNA in its canonical B-conformation causes a large axis bend and a rearrangement of DNA as experimentally observed in the platinated adducts, with NMR chemical shifts in qualitative agreement with the values in aqueous solution.[4,5]

Introduction

Cisplatin (*cis*-diamminedichloroplatinum(II)) is widely used in clinical treatment against a variety of cancer diseases.[6−11] Its beneficial effects arise from its binding to DNA nucleobases, preferentially to the two N7 atoms belonging to two adjacent G nucleobases or, to a lesser extent, to AG sequences.[12−14]

Cisplatin binding induces an overall curvature of the DNA double helix toward the major groove[1,3,7,15−21] associated with an opening of the minor groove. The platinated DNA moieties bind to the high mobility group (HMG) domains of proteins,[17,22−26] impeding replication and cell repair processes,[27] leading eventually to cell death.[6,8,15,16,28−31]

The available structures of cisplatin in complex with B-DNA oligomers (Table 1) in the solid state (solved by X-ray diffraction)[2,18] and in aqueous solution (solved by NMR)[3,19,32] have provided detailed information on the mode of binding of cisplatin. The metal ion, by binding to DNA, causes an axis bend of the double helix ranging from 40° to 84°.[1,3,7,18−20,33,34] Furthermore, the rise is larger and the propeller twists are larger at the platinated site than in the rest of the biomolecule,[35] and some of the Watson−Crick hydrogen bonds may be disrupted.[3,36] The minor groove opposite to the cisplatin lesion is deeper and shallower than in A-DNA.

A comparison between the X-ray[1] and NMR[3] structures of cispt-d(CCTCTG*G*TCTCC)-d(GGAGACCAGAGG) (**A**, Figure 1) has allowed the structural differences to be pinpointed on passing from the solid state to aqueous solution, namely, (i) an increase of the axis bend and roll angle; (ii) a decrease of the displacement of the Pt atom from the purine rings; (iii) a different puckering of the 3′-sugar at the platinated lesion, which is 3′-endo in the X-ray structure and 2′-endo in solution (Table 2). In the X-ray structure, the Pt-coordination geometry is slightly distorted from its typical square planar conformation: the metal ion moves out of the plane defined by the purine rings (deviations of 0.4−1.3 Å), with an N7−Pt−N7 angle as small as 69°.[37] The details of the Pt stereochemistry could not be detected in the NMR structure, and the planarity of the Pt structure has been imposed as a constraint.[38−40]

The structural basis of the molecular recognition between the HMG protein domain and the platinated DNA has been provided by the X-ray structure of a platinated 16-mer, cispt-d(CCU-CTCTG*G*ACCTTCC)-d(GGAGAGACCTGGAAGG) in complex with HMG A (**B**, Figure 1).[2] The structure shows that HMG A binds to the widened minor groove of the DNA duplex opposite to the cisplatin lesion. As a consequence, the roll angle and rise between the platinated guanines are even larger than in platinated DNA oligomers. The key structural determinants for sequence-specific molecular recognition by HMG[2] have been found to be the C25- and C24-PHE37 stacking interactions and the hydrogen bond between SER41 and the adenine base in the 3′-position of the cisplatin lesion (Figure 1SI).

Force-field based molecular dynamics simulations have provided complementary information on the dynamics and flexibility of cisplatin and other Pt-based drug−DNA complexes.[28,40] In particular, they have shown that platinated DNA structures are highly flexible, with large fluctuations of the axis bend of the double helix. On the other hand, the Watson−Crick

* To whom correspondence should be addressed. E-mail: carloni@sissa.it. Tel: +39 040 3787 407.
† SISSA.
‡ DEMOCRITOS.
§ EPFL.

10.1021/jp036230s CCC: $27.50
Published on Web 01/29/2004

TABLE 1: Available Structures of Cisplatin−DNA Complexes Where G* Denotes the Platinated Site

pdb-entry	experiment/resolution or #struct.	sequence	specification	axis bend [°]
1A2E[92]	X-ray/1.63	5′-d(CCTCG*CTCTC)- 5′-d(GAGAG*CGAGG)	interstrand	
1A84[3]	NMR/1	5′-d(CCTCTG*G*TCTCC)	intrastrand	84.5
1AIO[1]	X-ray/2.6	5′-d(CCUCTG*G*TCTCC)- 3′	intrastrand	39.7
1AU5[20]	NMR/1	5′-d(CCTG*G*TCC)	intrastrand	65.8
1CKT[2]	X-ray/2.5	5′-d(CCUCTCTG*G*ACCTTCC)	intrastrand HMG A	65.7
1DDP[93]	NMR/10	5′-d(GATAG*CTATG)- 5′-d(CATAG*CTATC)	interstrand	
1I1P[94]	X-ray/1.63	5′-d(CCCTCG*CTCTC)- 5′-d(GAGAG*CGAGG)	interstrand	
1KSB[19]	NMR/1	5′-d(ctccg*g*cct)	intrastrand	55.6
5BNA[95]	X-ray/2.6	5′-d(CGCG*AATTCG*CG)- 5′-d(CGCG*AATTCGCG)	monosubstituted	-

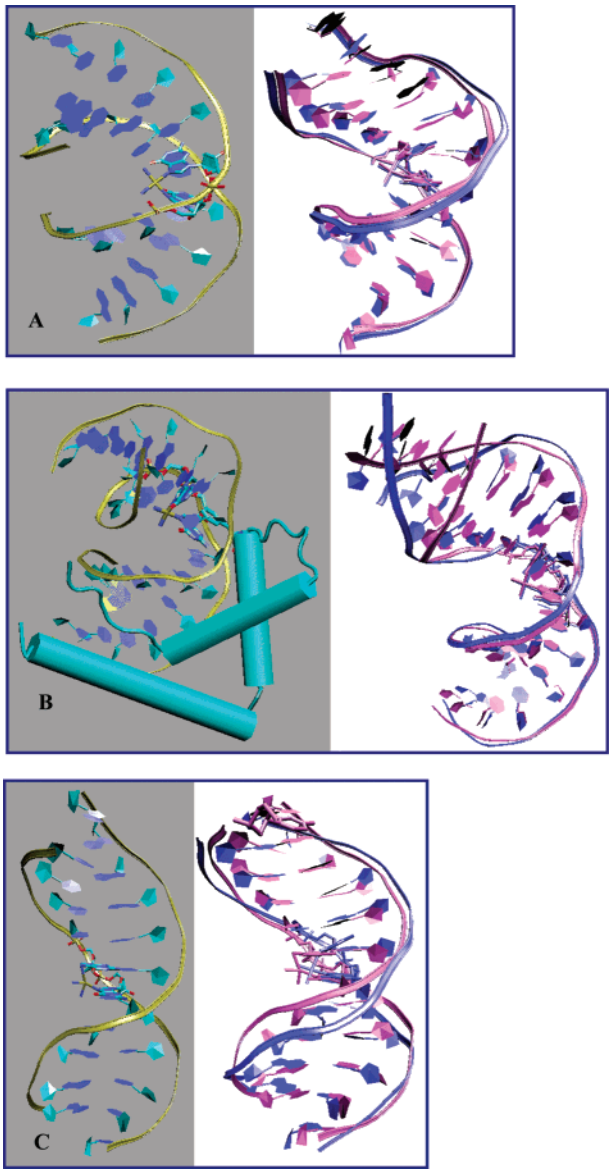

Figure 1. Complexes **A**−**C** used in the QM/MM calculations. The DNA oligomers are shown as ribbons, the cisplatin moiety and (in **B)** PHE37 and SER41 as sticks. In **B**, the protein is shown as a cartoon model. Left: Initial structural models [**A**, cispt-d(CCTCTG*G*TCTCC) -d(GGAGACCAGAGG), pdb-entry 1AIO[1]; **B**, cispt-d(CCUCTCTG*G*ACCTTCC)-d(GGAGAGACCTGGAAGG) HMG A domain complex pdb-entry 1CTK[2]; **C**, cisplatin moiety docked on an MD-equilibrated B-DNA structure]. Right: comparison between the initial (purple) and final QM/MM (blue) structures. In **B**, the protein is not shown for the sake of clarity.

H-bond pattern is completely maintained.[30,41] Due to the very specialized character of these parameters, the transferability of the force field models is limited.[39,42] For instance, the intrinsic dependence of platinum coordination on the electronic structure requires a special set of torsional parameters to be introduced in the force field.[38] As a result, force field parameters are only available for very few Pt-based ligands.[38−40,43−45] In this respect, a quantum chemical, parameter free approach for the metal-containing moieties in combination with well-established potentials for the macromolecular frame could be useful to extend the domain of applications in platinum/DNA chemistry.[46,47]

Here, we present hybrid quantum-mechanical/molecular mechanics simulation studies on cisplatin/DNA complexes.[3,7,16,18−20,34,41,48,49] Our approach allows for a density functional treatment of the platinum moiety along with a classical mechanics treatment of the molecular frame and solvent[50,51] that takes the steric and electrostatic effects of the surrounding explicitly into account. The first-principles calculations are carried out with the Car-Parrinello approach,[52] which has proven to reliably describe structure, dynamics, and electronic properties of platinum−nucleotide complexes in the solid state[53] as well as in water solution.[49]

Our calculations are based either on the X-ray structures of platinated DNA (**A**[1], Figure 1 and **B**[2], Figure 1) or on a cisplatin docked B-DNA structure (**C**, Figure 1).

A turns out to rearrange significantly, and at the end of the dynamics, it features structural properties fairly similar to those of the NMR structure in solution.[3] In particular, the geometry of the Pt complex is coplanar, and the axis bend of the structure passes from 39° to 51°, which is still lower than in the experiment (84°).[3] The calculated ^{195}Pt NMR data, which are very sensitive to structural changes, such as bond lengths and distortions of the square planar coordination geometry,[54,55] are in qualitative agreement with the experimental data.

B, in complex with HMG A, on the other hand turns out to keep its structure similar to that of the X-ray data, as expected for a protein/DNA complex, which is more rigid than DNA alone.

Our computational approach is finally used as a predictive tool by docking cisplatin to B-DNA (**C**, Figure 1). Within the short time scale investigated (7 ps), the metal induces a distortion in our complex that is similar to that of **A**, with an axis bend of ∼48°.

Methods

Structural Models. The calculations were based on the three structures shown in Figure 1: (**A**) cisplatin-d(CCTCTG*G*TCTCC) X-ray structure at 2.6 Å resolution (pdb-entry 1AIO[1]). (**B)** cisplatin-d(CCUCTCTGGACCTTCC)/HMG1 A domain X-ray structure at 2.5 Å resolution (pdb-entry 1CKT[2]). The positions of 71 out of 89 residues of HMG1 structure have been detected. The two histidine residues (HIS20 and HIS24) present in the structure were assumed to be protonated on the δ-N atom based on their putative hydrogen-bonding pattern. (**C)** Cisplatin docked onto MD equilibrated d(CCTCTGGTCTCC)-B-DNA (**C0**, Figure 2SI).

TABLE 2: Selected Structural Parameters Describing Pt-Coordination Geometry and DNA Structure[a]

	A	**B**	**C**	X-ray[1]	X-ray HMG[2]	NMR[3]
DNA base parameters						
rise G6-G7 [Å]	4.3	7.7	5.0	3.5	7.7	5.7
roll angle [°]	42 (9)	61 (7)	28 (8)	29	64	46
overall axis bend [°]	51 (10)	57 (5)	48 (8)	40	66	85
buckle T5-A20	1 (11)	9 (11)	−9 (11)	7	11	−2
buckle G6-C19	9 (12)	44 (9)	18 (9)	14	29	33
buckle G7-C18	−6 (9)	−21 (11)	−2 (9)	−2	−13	−0
buckle T8-C18	6 (10)	−6 (8)	12 (10)	−3	4	20
propeller T5-A20	−14 (11)	1 (10)	−2 (9)	−7	3	30
propeller G6-C19	−34 (13)	−6 (10)	−18 (10)	−24	−1	−7
propeller G7-C18	−16 (11)	5 (9)	−12 (11)	−16	20	−9
propeller T8-C18	−11 (13)	−9 (11)	−11 (9)	−30	2	−3
Pt-coordination geometry						
Pt−N7(G6*)	2.06 (0.07)	2.02 (0,15)	2.07 (0.06)	1.91	1.98	1.94
Pt−N7(G7*)	2.03 (0.06)	2.00 (0.14)	2.07 (0.04)	1.90	1.89	1.89
Pt−N(AM1)	2.11 (0.06)	2.09 (0.15)	2.07 (0.02)	1.89	1.98	1.98
Pt−N(AM2)	2.09 (0.06)	2.08 (0.15)	2.08 (0.03)	1.96	1.96	1.92
N7−Pt−N7	86 (3)	89 (3)	86 (3)	100	90	90
AM1-Pt-AM2	89 (5)	91 (4)	92 (3)	92	89	90
N7−Pt-AM1	90 (5)	92 (5)	89 (4)	88	89	90
N7−Pt-AM2	93 (5)	88 (4)	93 (4)	72	92	90
displ. of Pt from G6*	0.8 (0.1)	0.4 (0.1)	0.74 (0.1)	1.3	0.48	0.7
displ. of Pt from G7*	0.34 (0.1)	0.09 (0.1)	0.8 (0.1)	0.8	0.0	0.64
torsional angles						
G6* χ	−149 (9)	−98 (10)	−80 (10.5)	−147	−108	−109
G6* δ	82 (8)	91 (9)	132 (11)	91	105	92
G6* ζ	−54 (11)	−64 (9)	−84 (42)	−56	−81	−29
G7* χ	−149 (14)	−113 (15)	−126 (15)	−168	−110	−141
G7* δ	85 (13)	140 (10)	107 (19)	82	137	136
G7* ζ	−76 (11)	−103 (60)	−98 (16)	−82	−148	−91
sugar puckers						
G6*	C3′-endo	C2′-exo	C2′-endo	C3′-endo	C3′-endo	C2′-exo
G7*	O1′-endo	C2′-endo	O4′-endo	C4′-exo	C2′-endo	C2′-endo

[a] Distances are given in angstroms, and angles, torsional angles, buckling, and propeller twists are in degrees. Standard deviations are given in parentheses.

Sodium counterions were added so as to counterbalance the total charge of **A**−**C0**: the ions were located in the positions of lowest electrostatic potential, calculated with the AMBER electrostatic term.[56] These complexes were immersed in a periodic box filled with water molecules, at a density of 1.0 g/cm^3. Water molecules with their oxygen atoms closer than 1.76 Å (i.e., the van der Waals radii of oxygen) to any atom of the complex were discarded. The final number of atoms and the sizes of the simulation boxes are reported in Table 1SI.

MD Calculations. All structural models underwent first an equilibration phase via classical MD, carried out with the AMBER6 program package.[56,57] The AMBER parm98 force field[58,59] was adopted for DNA, the HMG A domain, and the sodium counterions. For $[Pt(NH_3)_2$-d(G*G*)$]^{2+}$ and the guanine bases, the parametrization of Herman et al. was used[38] along with a harmonic constraint of 5 kcal/(mol·Å^2) on all the atomic positions of the cisplatin moiety $[Pt(NH_3)_2$-d(pG6*pG7*)] and, in **B,** on C24, C25 nucleobases and residue PHE37. The latter constraint turned out to be necessary to avoid unphysical distortions of these groups. Because the van der Waals parameters of Pt were not reported in ref 38, they were taken from ref 40, which models Pt/DNA complexes in vacuo. Test calculations showed that with these parameters water molecules at times penetrated the metal coordination sphere (distance Pt−O < 3 Å, Figure 6SI), in contrast to the results of ab initio calculations. Thus, the van der Waals radius of platinum was increased from 2.4 to 2.8 Å. Solvent water molecules were treated with the TIP3P model.[60] Electrostatics were evaluated with the particle mesh Ewald (PME) method.[61] A cutoff of 10 Å was used for the van der Waals interactions and the real part of the electrostatic interactions. A time step of 1 fs was applied. Room-temperature simulations were achieved by coupling the systems to a Berendsen thermostat.[62] The initial structures were relaxed by short steepest descent minimization runs of 1000 steps. 100 ps MD at constant volume were performed during which the system was heated to 300 K.

2 ns of MD at constant pressure (1 atm) and temperature (300 K) were then performed. The final MD structures of the models, which are shown in Figure 3SI, exhibited an overall rmsd of 3.2 (**A**), 1.8 (**B**), and 3.0 Å (**C0**) with gyration radii of 11.5 (**A**), 10.2 (**B**), and 11.5 (**C0**) and final densities of the system of 1.05, 1.03, 1.02 g/cm^3, respectively.

No significant rearrangement was observed during the dynamics (Figure 3SI). In particular, in **C0**, 13 sugar puckers kept their C2′-endo conformation, whereas the other sugars were in the closely related C1′-exo conformation.

QM/MM Calculations. The CPMD program[52] combined with classical MD, based on both GROMOS96[63] and AMBER force fields,[58,59] through the interface developed by Rothlisberger et al., was used.[50,51,64] The final **A**, **B**, and **C** MD structures were partitioned into two regions. The first region was treated at the quantum mechanical level (QM hereafter, Figure 2, Table 2SI); the second was treated classically (MM hereafter). The quantum atoms, which are linked by a covalent bond to the classical part of the system were saturated by positionally unrestrained, additional "capping" hydrogen atoms[65] (Table 2SI). Quantum-chemical calculations were carried out within the framework of density functional theory. To check the dependency of the electronic structure of the metal ion on the choice of our QM system, a single-point calculation with an extended QM system, including also T5, T8, C18, and C19, was performed. The Pt electronic structure exhibits no significant changes (data not shown). The basis set consisted of plane waves (PW) up to an energy cutoff of 70 Ry. Core/valence interactions

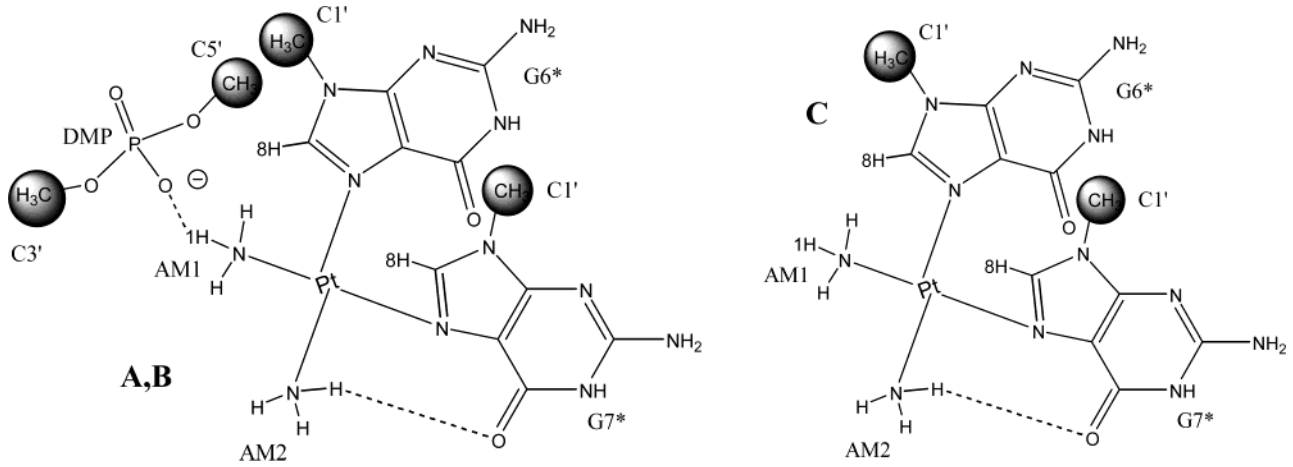

Figure 2. QM regions in models **A**−**C**. Hydrogen bonds are indicated with dotted lines. Capped atoms are indicated by gray spheres.

were described using norm conserving pseudopotentials of the Martins-Troullier type.[66] Integration of the nonlocal parts of the pseudopotential was obtained via the Kleinman-Bylander scheme[67] for all of the atoms except platinum, for which a Gauss-Hermite numerical integration scheme was used. The gradient corrected Becke exchange functional and the Lee−Yang−Parr correlation functional (BLYP) were used.[68,69] Isolated system conditions[70] were applied. D-RESP charges were calculated at each MD step as described in ref 50. In all complexes, the QM/MM-averaged charges are lower in absolute value than the values in the parametrization of Herman,[38] possibly because of the presence of the DNA environment (Table 3SI). The MM region was described with the AMBER force field.[58;59] The electrostatic interactions between QM and MM atoms were calculated using a hierarchical scheme.[51] In this approach, the short range electrostatic interactions between the QM and MM part were taken explicitly into account within a sphere of radius 5.3 Å around every QM atom using an appropriately modified Coulomb potential that ensures that no electron spill-out occurs. Beyond this first shell and within 10.6 Å, the electrostatic interactions were calculated using the D-RESP charges[50] for the QM atoms. In the outermost region, a multipole expansion scheme was employed. This hierarchical method is fully Hamiltonian and ensures high accuracy in the core region and efficient computation in the region further away from the QM part.

For the three systems, the MM regions were first relaxed during 1000 steps of MD, while keeping the QM part frozen. Then 1000 steps of simulated annealing were performed on the QM system in order to relax the constraints on the QM atoms. The systems were slowly heated to 300 K. A time step of 0.073 fs was used. NVT simulations were carried out by coupling the systems to a Nosé-Hoover thermostat.[71;72] The distance constraints between N(AM1)-O1P(DMP) and N7(G6*)-N7(G7*) were applied in model **A** and **B** during the heating (Figure 2) and released when room temperature was reached. In model **C**, the annealing procedure was repeated several times, decreasing step by step the distance between Pt and N7 from 2.5 Å to a final value of 2.17 Å. Then the system was heated while the distance between the Pt and N7 atoms was kept fixed. At 300 K, the constraints were released. The simulations cover 5ps (**A** and **B**) and 7ps (**C**), respectively.

Property Calculations. *(i) Structural Properties*. Sugar puckers, torsional angles, and helix bending are defined according to the EMBO Workshop on DNA Curvature and Bending.[73] They were calculated using the program Curves 5.1.[74,75] Radial distribution functions ($g(r)$) were calculated using the ptraj module of the AMBER6 package.[57] *(ii) Electronic Properties*. Energy levels of HOMO and LUMO were calculated by diagonalization of the Kohn−Sham states both on the QM regions of complexes **A**-**C** and of gas-phase models of cisplatin (Figure 4SI) in different conformations. *(iii) ^{195}Pt Chemical Shifts*. The ADF code[76−78] with a localized, Slater-type basis set (STB) was used. A triple-ζ basis set with one polarization function (TZP) for Pt and a double-ζ basis set with one polarization function (DZP) for the other atoms along with the BP approximation[68,79,80] of the exchange correlation functional were used. The BP functional is known to be more accurate than the BLYP approximation for the NMR properties, in particular for heavy atoms.[81,82] Scalar relativistic effects are taken into account with the zero order regular approximation (ZORA) approach.[54;81−84] Test calculations on cisplatin and $[Pt(NH_3)_2(C_3H_4N_2)_2]^{2+}$ ([cispt-(imidazole$_2$)]$^{2+}$, Figure 4SI) were performed to estimate the effect of distortions on the calculated chemical shift (Table 4SI). It was found that the latter is very sensitive to bond lengths but to a lesser extent to a distortion of the angles and out of plane displacement of the metal ion. The ^{195}Pt chemical shifts, which are calculated on selected snapshots of the CPMD/classical MD trajectory, are expected to experience extremely large variations, because of the fluctuations of the Pt-ligand bond lengths during the dynamics (Table 4SI). Thus, calculations can provide only qualitative results here.

Notice that spin−orbit terms[82] account for ≈10% of the chemical shift, as shown by test calculations on the cisplatin molecule and cisplatin-guanine complexes $[Pt(NH_3)_2G_2]^{2+}$. Indeed, as already discussed previously,[54] the ^{195}Pt chemical shift is mainly determined by the paramagnetic contribution.[83] Thus, these terms are not expected to affect significantly the results and they were not included here because of their large computational cost.

The difference between these chemical shifts and that of cisplatin in water (geometry taken from the MD-averaged structure of ref 49) were finally calculated.

Calculations on Model Complexes. The effect of the distortion on the metal stereochemistry induced by the DNA in the experimentally determined structure **A** was evaluated by performing DFT calculations in vacuo on cisplatin and imidazole containing Pt complex $[Pt(NH_3)_2(C_3H_4N_2)_2]^{2+}$ (Figure 4SI).

BLYP−PW[68] calculations were carried out using the same computational setup as above. In addition BLYP−STB and BP[68]-STB calculations were carried out in order to check the dependence of the relative energies on the basis set and exchange correlation functionals. These calculations used a double-ζ basis set with polarization functions for all of the atoms. The core electrons were frozen up to 4f for Pt, 2p for Cl, and 1s for N.

TABLE 3: Electronic Properties of (a) Cisplatin and $[Pt(NH_3)_2(N_2C_3H_4)_2]^{2+}$ (Figure 4SI) and (b) Complexes A−C[a]

(a)	I	II	III	IV	V
		Geometry			
Pt−Cl [Å]	2.34	2.35	2.36	2.05	2.05
Pt−N [Å]	2.10	2.12	2.10	2.09	2.09
Cl−Pt−Cl [°]	96	93	76	88	88
N−Pt−Cl [°]	83	82/83	94/96	91	91
N−Pt−N [°]	98	96	94	90	90
out of plane[b] [°]	0	29.3	2.8	0.0	0.0
Displ. purine				0.0	0.8
		HOMO−LUMO Energy Gap [eV]			
CPMD	2.826	2.478	2.672		
ADF	2.667	2.306	2.490	3.42	3.38
		^{195}Pt NMR Chemical Shift with Respect to Cisplatin in Vacuo ADF			
	0			287	350

(b)	A	B	C
	HOMO−LUMO energy gap [eV]		
CPMD	2.4	2.6	3.0
ADF	2.3	2.3	2.3
	^{195}Pt NMR Chemical Shift with Respect to Cisplatin in Vacuo		
ADF	637 (353)	534 (243)	532 (140)

[a] In (a), I refers to the fully optimized structure in vacuo, II to the optimized structure with the "out of plane" conformation of the X-ray structure,[1] III to the optimized structure with Cl−Pt−Cl angle as in the X-ray structure,[1] IV to the $[Pt(NH_3)_2(N_2C_3H_4)_2]^{2+}$ optimized structure, and V to $[Pt(NH_3)_2(N_2C_3H_4)_2]^{2+}$ optimized structure with the Pt displaced from the imidazole ring as in the X-ray structure. [b] Distortion is measured as the angle between the two planes spanned by the atoms Cl−Pt−Cl and N−Pt−N.

For platinum, scalar relativistic effects were taken into account by using the zero order regular approximation (ZORA).[82] The complexes underwent (i) full geometry optimization, (ii) optimization with the "out of plane" conformation of the X-ray structure,[1] and (iii) optimization with the Cl−Pt−Cl angle fixed to the value of the X-ray structure (Figure 4SI). [1] The energetics using PW and STB basis sets turned out to differ by less than 6% (Table 3).

Results and Discussion

QM/MM calculations are carried out with a platinated DNA dodecamer[1] (A, Figure 1) and a platinated 16-mer in complex with the HMG domain (B, Figure 1), based on the X-ray structures determined by Lippard and co-workers.[2] The calculations were preceded by 2.0 ns classical MD simulations allowing for a relaxation of the DNA structure, while keeping the cisplatin moiety close to its initial position. Comparison is made with NMR structural data and with ^{195}Pt chemical shifts of cisplatin−DNA adducts.[4,5] This section is concluded by a docking of the $[Pt(NH_3)_2]^{2+}$ moiety on a B DNA dodecamer (C, Figure 1) and subsequent QM/MM simulation.

Results for Complex A. The average axis bend increases to an intermediate value between that in the X-ray structure and that in the NMR-structure (Table 2). During the short time scale explored, the axis bend covers values from 30° to 76°. Also the roll angle varies considerably with an increasing trend toward the roll angle of the solution structure (Table 2).[18] The QM/MM averaged values of the key backbone torsional angles are reported in Table 2 and Table 4SI. The experimentally observed repuckering from A-DNA in the solid state to B-DNA in aqueous solution occurs on a time scale of 200−500 ps.[59,85] Here, as expected, it is not observed during our simulation time.

TABLE 4: rmsd Values [in Å] of Complexes A−C and in the NMR Structure of Ref 3[a]

	A	B	C	NMR struct.
A	0.9/1.8	1.04/-	0.9/2.98	1.50/4.20
B		0.80/1.8	1.16/-	1.32/-
C			1.34/2.02	1.47/3.96

[a] The first value refers to the Pt moiety as shown in Figure 8SI, and the second value refers to the entire double helix. rmsd between the same structures refer to the initial and final QM/MM structure.

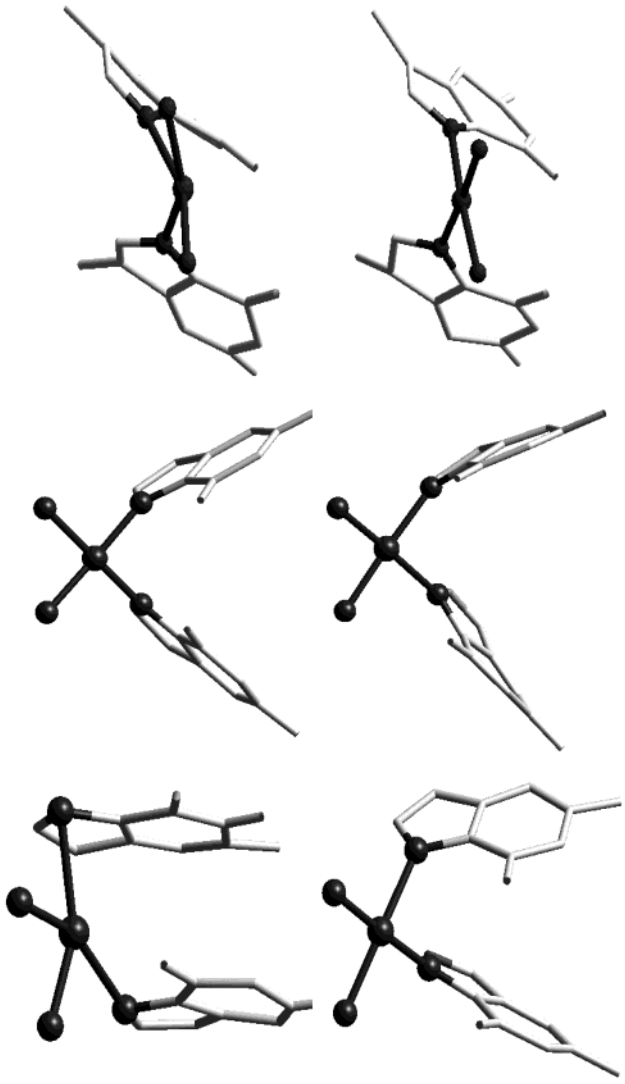

Figure 3. Starting (left) and final (right) structure of QM regions for model **A**−**C.** Upper panel, **A**. Middle, **B**. Lower panel, **C**.

The platinated site is structurally similar to the initial structure (rmsd: 0.9 Å, Table 4). However, the Pt-ligand distances are slightly longer than in the X-ray or in the NMR structure, as already noticed in calculations with this computational setup.[49] The platinum ion, which is moved out of the square planar coordination plane in the X-ray structure, lies now in the plane defined by its four ligands (Figure 3). The displacement of the metal ion from the purine ligands is smaller than in the X-ray structure. It is instead rather similar to that in the NMR structure of the same molecule in water (Table 2).

The distortion of the Pt−N7-purine ring angle is known to be related to the destacking of the G6*G7* bases:[3] a larger roll angle between the platinated residues allows for a less distorted Pt-coordination geometry,[2] favoring in this way complex formation. On the other hand, because of the increased roll angle,

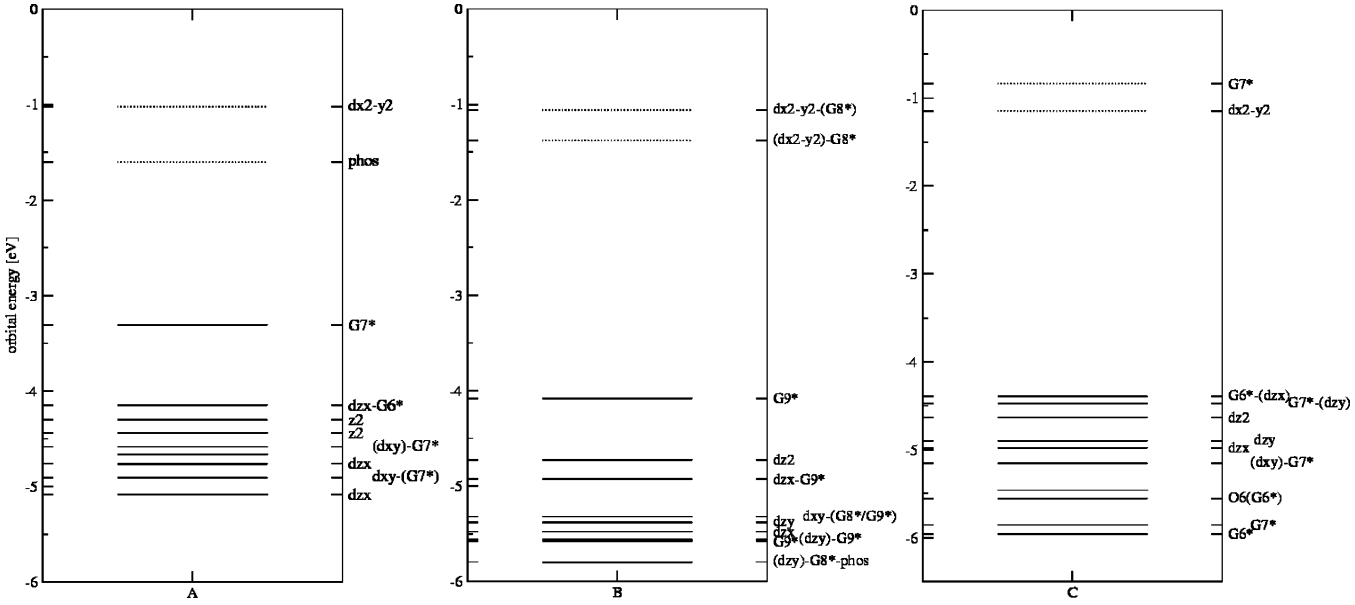

Figure 4. Energy level diagram around the HOMO−LUMO gap complexes **A**−**C**.

the hydrophobic bases are more solvent exposed than in undistorted B-DNA. Consistently, in our final QM/M structure, the N7−Pt−N7 angle increases from 77° in the X-ray structure to 86° (Table 2) and the roll angle is 42° (Table 2).

To estimate the effect of these distortions on the electronic structure and on the energetics, we carry out calculations on model systems, namely cisplatin and the imidazole containing complex $[Pt(NH_3)_2(C_3H_4N_2)_2]^{2+}$ in vacuo (Figure 4SI). Different conformations, with geometries similar to that of the $[Pt(NH_3)_2$−d(G6*G7*)$]^{2+}$ geometry in the X-ray structure, are compared to the fully optimized geometries (see the Methods section). The energy of the molecule on passing from the "out of plane" conformation, as observed in the X-ray structure,[1] to the optimized geometry is 8.0 kcal/mol. [With a localized basis set, we obtain an energy difference of 8.3 kcal/mol.] Such an energy barrier suggests that the "out of plane" conformation found in the X-ray structure has a very low probability. However, environmental effects, which are neglected in these calculations, could alter significantly this picture. In addition, removal of this distortion causes an increase of the HOMO−LUMO gap from 2.5 to 2.8 eV. Distortion of the Cl−Pt−Cl angle has a much less significant effect (Table 3, Table 4SI). In all conformations, the HOMO is mainly localized on the corresponding metal d_{xy} orbital, as in the geometry-optimized structure,[53] and the LUMO is on the $d_{x^2-y^2}$ orbital, which is to be expected for a d^8 diamagnetic square planar complex. The distortion causes also a slight elongation of the metal−ligand bonds (Table 3). The same holds true for a displacement of the Pt atom from the imidazole rings.

The presence of the biomolecular frame modifies the nature of the chemically relevant orbitals. In the QM region of complex **A**, the HOMO lies in the π-system of G7*, whereas the LUMO is localized on the phosphate group (Figure 4). The HOMO−1 corresponds to the d_{xz} orbital, but all of the d-levels are clustered within 1 eV. The $d_{x^2-y^2}$ level, on the other hand, is shifted to the LUMO+1 level. Reordering of the electronic energy levels is probably due to the perturbation by O6 of the guanine ligands (isodensity surfaces are shown in Figure 5SI) and has already been observed in Pt-nucleotide complexes.[49]

The ammonia (AM1, Figure 2)−G6 phosphate hydrogen bond, present in the X-ray structure, is first broken and then reformed several times until, after about 3 ps, it is definitively lost. This feature may be consistent with the NMR structure of the complex in solution, which does not exhibit this H-bond.[3] The relatively weak AM2-O6(G7*) H-bond, present in the X-ray and NMR structure, is instead fully conserved during the dynamics. The other hydrogens belonging to the two ammonia ligands form H-bonds with water molecules (treated classically). In the first solvation shell, there are on average 2.8 water molecules (Table 5, Figure 6SI).

Figure 5. Superposition between **A** (blue) and **C** (orange).

TABLE 5: Number of Water Molecules in the First Solvation Shell around the Ammonia Ligands (within 3.5 Å) and around Pt (within 5.0 Å)

	A	B	C
AM1	2.8	4.3	4.2
AM2	2.3	3.4	3.4
Pt	6.1	8.3	8.8

The ^{195}Pt NMR chemical shift relative to the cisplatin in vacuo with the average MD structure is 637 (±353) ppm, as compared to the experimental value of ~310 ppm[4] (Table 3, Figure 7SI).[5] Typical errors in calculated ^{195}Pt chemical shifts for *energy-*

minimized square planar complexes involving Cl and N ligands range from 30 to 160 ppm.[83] The larger error found here (over 300 ppm) might be at least in part caused by the fact that the calculations are based on QM/MM snapshots where bond lengths are highly fluctuating. This in turn dramatically affects the ^{195}Pt NMR chemical shifts (Table 5SI) so that only qualitative agreement with experimental values is obtained. The Watson−Crick hydrogen bond between the platinated GC pair, namely G6*−C19, which is intact in the X-ray structure, breaks and reforms several times. This feature may be consistent with the NMR data, which indicate that the G6*−C19 base pair is perturbed, retaining only the G6*(O6)−C19(N4) hydrogen bond.[3] The simulation suggests that also the G7*−C18 base pair is highly flexible and the Watson−Crick H-bond is broken and reformed several times. This bond is intact in the solution structure but distorted in the crystal structure.[1] Propeller twists are increased with respect to standard B-DNA, having values as high as 30° (Table 2). Finally, the minor groove width at the platinated site ranges from 8.3 to 8.7 Å and is thus slightly narrower than in the crystal structure and the solution structure (Table 4SI). The final rmsd of complex **A** with respect to the initial crystal structure and the NMR structure is 1.8 and 4.0 Å, respectively, including all atoms. When considering only the Pt-moiety the rmsd is 0.9 and 1.5 Å for the X-ray structure and NMR structure, respectively (Table 2).

Results for System B. The overall axis bend in the DNA decreases slightly during the simulation from 66° to 57°. Its roll angle is 61° similar to the X-ray structure (Table 2). The rise at the G8*G9* step is significantly larger than in complex **A** (7.7 Å) and in fair agreement with the crystal structure (7.4 Å). The destacking of the two bases leads to a smaller distortion of the Pt−N7 bond[2]: the displacement of the Pt atom from the purine planes is smaller than in **A**. On the other hand, the hydrophobic faces of the guanine bases are even more solvent exposed than in **A** (Figure 8SI). The sugar puckers and the Watson−Crick H-bond patterns are maintained (Table 2 and Table 4SI). In terms of torsional angles, the structure has B-DNA character except for G8* and C11, which exhibit A-DNA character (Table 2 and Table 4SI). G8*, binding to Pt in the 5′ position, has A-DNA conformation also in the X-ray structure,[2] but C11 has B-DNA character in the X-ray structure. The repuckering could be due to thermal fluctuations. The minor groove width and depth are similar to those of the initial X-ray structure.[2] The initial platinum coordination geometry, which is less distorted than in the X-ray structure of the platinated DNA in the free state (Table 2), is well maintained. The Pt atom lies in the square planar coordination plane in agreement with the X-ray structure (Table 2). The HOMO lies mainly in the π*(G9*) system as in **A**, whereas the HOMO−1 is concentrated in the d_{z^2}-metal orbital (Figure 4, isodensity surfaces in Figure 5SI). The latter is destabilized due to the almost axial position of the O6(G9*) oxygen with respect to the Pt-coordination plane (Figure 5SI). Again, the d levels are clustered within 1 eV. The LUMO lies on the $d_{x^2-y^2}$ orbital (isodensity surfaces in Figure 5SI). The hydrogen bond between the phosphate group of G8* and AM1 is lost at the beginning of the dynamics, when the restraint is released, whereas the N(AM1)−O6(G8*) and N(AM2) and O6(G9*) hydrogen bonds are maintained. In contrast to **A**, all three hydrogen atoms of AM1 are able to form hydrogen bonds to the solvent, and therefore, there are more water molecules in the first solvation shell than in complex **A** (Table 5). There are more than three waters in the first solvation shell of AM1. As mentioned in ref 86, this feature is due to the presence of mobile water molecules in the first solvation shell, which are not directly hydrogen bonded to ammonia. AM2 has less water molecules in its first solvation shell than AM1 since one hydrogen is involved in a hydrogen bond toward O6 of G9*.

C: Docking of $[Pt(NH_3)_2]^{2+}$ on B-DNA. The predictive power of our computational setup was investigated by constructing a structural model of platinated DNA. The $[Pt(NH_3)_2]^{2+}$ moiety was docked onto the two adjacent guanines of B-DNA with the same sequence as **A.** The B-DNA structure in solution was previously equilibrated by 2 ns of classical dynamics.

The initial Pt-coordination geometry after docking is highly distorted (Figure 1 and Figure 2SI). The initial N7−Pt−N7 angle is 135° and the initial N7−Pt bond lengths are fixed to 2.5 Å. The stabilization energy due to relaxation of the system, calculated by comparing the energy of the $[Pt(NH_3)_2G_2)]^{2+}$ moiety in its initial and final structure, is as high as ∼150 kcal/mol. Most of this energy resides in the rather strong coordination bonds.[46] During the simulation, the N7−Pt−N7 angle decreases and the roll angle between G6* and G7* increases (Table 2). The final value is still below the one of **A**, but the running average shows an increasing trend (data not shown). The distortion induced by the cisplatin moiety affects the overall structure and readily leads to an axis bend in the double helix. The average axis bend is 48° (±8°), which is still lower than in the reported NMR structure,[3] but the values range from 30° to 65° during our simulation. The torsional angles and sugar puckering are maintained (Table 2 and Table 4SI). The square planar coordination geometry is slightly more distorted than in **A**, as shown by the displacement of the Pt atom from the purine ring planes (Table 2). The calculated HOMO and LUMO gap is slightly larger than in complex **A.** The HOMO has large parts of the density on the π system of the guanine ligand, whereas the LUMO corresponds to the $d_{x^2-y^2}$ (Figure 4, isodensity surfaces shown in Figure 5SI) as in **B**. The d levels lie just below the HOMO clustered within 1 eV. The ^{195}Pt NMR chemical shift relative to cisplatin is 532 (±116) ppm, also in this case in qualitative agreement with experiments.[4,5] The very large standard deviations do not allow establishing whether the agreement is better here or in complex **A**. The AM1 ammonia ligand does not interact with the phosphate group of G6* during the duration of the QM/MM simulation, and the distance between the groups decreases from 9 to 7 Å, which corresponds to an indirect hydrogen bond, mediated by two water molecules. Classical MD simulations have shown several transitions from a direct phosphate−AM1 hydrogen bond to a water mediated hydrogen bond[41] as observed when passing from crystal[1] to solution structure.[3] During a very short interval in the MD dynamics[41] also the two water mediated hydrogen bond has been observed as in **C**. A direct hydrogen bond favors however the N conformation of the sugar in 5′-position of the Pt-lesion, whereas with increasing distance between AM1 and the phosphate group, the S conformation becomes accessible as well. The hydrogen bond between AM2 and O6 of G7* is present as in complexes **A** and **B**. AM1 solvation properties are similar to that of **B** (Table 5). The Watson−Crick hydrogen bonds are not disrupted during the simulation. The propeller twists between central base pairs are significantly lower than in complex **A** (Table 2). The structure maintains overall B-DNA character and is less distorted than complex **A**. The final structure is quite similar to complex **A** with an rmsd of 0.9 Å including the atoms at the Pt-site, and 3 Å including all atoms (Table 2). The main structural differences include the sugar ring of G6* and the G6*-phosphate group (Figure 8SI). The latter is located further away from the AM1 ligand than in complex **A**. The rmsd of complex

C with respect to the solution structure is 1.5 Å at the platinated site and 4.0 Å, including all atoms. Thus, the final **A** and **C** structures, even though generated from rather different structures, are in fair agreement with each other.

Final Remarks

We have presented a mixed quantum/classical simulation of cisplatin binding to DNA in the free state and in complex with HMG A (Figure 1).

In **A**, the coordination geometry of the cisplatin moiety changes significantly during the QM/MM simulation, which is based on the X-ray structure. The angle spanned by the two purine bases and the platinum increases on average by 10°. The Pt atom is now displaced from the purine ring planes by 0.8 and 0.4 Å respectively, comparable to the solution structure.[3] The axis bend increases from 39° to 51°, showing high flexibility even in the short time scale investigated. A hydrogen bond between one of the Pt-ammonia ligands and a phosphate group is broken, which is consistent with the experiment where the same H-bond is lost when passing from solid state[1] to solution.[3] A hydrogen bond between the other ammonia group and O6 of G6* is maintained, even though intuitively weaker than the other hydrogen bond. In agreement with the observed hydrogen bond pattern, the first ammonia ligand AM1 has more water molecules in its first solvation shell than the second ammonia AM2, which maintains its hydrogen bond to the guanine ligand. Our simulation suggests as well that the DNA double helix is flexible enough to maintain Watson−Crick hydrogen bonding even in a highly distorted structure such as the one present here. The sugar repuckering experimentally observed on passing from the solid state[1] to the solution structure[3] is not seen during the simulation, possibly because of the characteristic time scale of this event, which is longer than the simulation time. The calculated ^{195}Pt chemical shifts are only in qualitative agreement with those in water solution.

In **B**, the structure remains very close to the X-ray structure, in part because crystal packing effects play a minor role. The binding of the HMG A domain leads to a higher axis bend.[20] Still, as in **A**, the DNA maintains its high flexibility. The DNA adopts a larger rise and roll angle between the platinated guanines relative to complex **A**. As a result, the displacement of the Pt atom from the purine rings is lower and the Pt-coordination geometry is less strained than in complex **A**. Nevertheless, the two structures compare well, given that the orientation of the two guanine ligands is the same (Figure 8SI).

The DNA environment destabilizes the d_{zx} and d_{z^2} orbitals, leading to a reordering of the d levels with respect to cisplatin. Furthermore, orbitals involving the π system of the guanine ligands are close in energy, and we observe, indeed, that the HOMO has most of its density on the ligand π system. That the presence of the nucleobases alters significantly the electronic structure has already been seen in platinum−nucleotide complexes.[49] The electronic gap between HOMO and LUMO is decreased by 0.3−0.5 eV with respect to cisplatin in water due to the distortion assumed upon binding to the DNA and the high lying guanine π orbitals.

The predictive power of our computational setup is explored by docking the $[Pt(NH_3)_2]^{2+}$ moiety onto the two adjacent guanine nucleobases in canonical B-DNA structure. Despite the short time-scale investigated, the docking process causes a rather dramatic change in the DNA structure: The axis bend, the roll angle and the rise, although still out of range of the corresponding NMR structure,[3] increase toward the values of **A** and the solution structure and are still increasing in the end of our simulation (Table 2). The stabilization of the platinum complex from the initial, highly distorted structure to the final structure is rather large and is mostly caused by the increased Pt−guanine bond length.

We also attempted to calculate ^{195}Pt chemical shifts. The final results are only in qualitative agreement with experimental data,[4,5] and the too large errors in our data do not allow a structural relationship to be established.

We conclude that the QM/MM approach described here proves to be a valuable tool for metal−DNA models as well as classical molecular dynamics simulation.[38,39,41,43−45] It allows for a parameter free treatment of the metal-coordination geometry within the full DNA−solvent environment treated classically, and it can be used in the future to model the interaction of other platinum-based compounds with DNA oligomers and DNA nucleobases,[87−91] for which a valuable force field parametrization has not yet been developed.

Acknowledgment. This work was performed in the frame of the COST D20 project. Financial support from MURST COFIN is acknowledged.

Supporting Information Available: (i) Sizes of all classical MD and QM systems, (ii) D-RESP charges of QM/MM systems, (iii) ^{195}Pt chemical shifts for cisplatin model complexes, (iv) figure depicting protein-DNA interaction in complex **B**, (v) figure showing $[Pt(NH_3)_2]^{2+}$ docking on model **C0**, (vi) figure of initial and final classical MD structures and RMSD, (vii) cisplatin model complexes, (viii) visualization of HOMO and LUMO orbitals for QM/MM systems, (ix) radial distribution function around Pt-moiety, (x) running average of ^{195}Pt chemical shift for complex **A**, (xi) superposition of Pt-moiety for complexes **A**−**C** and the solution structure. This material is available free of charge via the Internet at http://pubs.acs.org.

References and Notes

(1) Takahara, P. M.; Rosenzweig, A. C.; Frederick, C. A.; Lippard, S. J. *Nature* **1995**, *377*, 649−652.

(2) Ohndorf, U. M.; Rould M. A.; He, Q.; Pabo C. O.; Lippard, S. J. *Nature* **1999**, *399*, 708−712.

(3) Gelasco, A.; Lippard, S. J. *Biochemistry* **1998**, *37*, 9230−9239.

(4) Bancroft, D. P.; Lepre, Ch. A.; Lippard, S. J. *J. Am. Chem. Soc.* **1990**, *112*, 6860−6871.

(5) Miller, S. K.; Marzilli, L. G. *Inorg. Chem.* **1985**, *24*, 2421−2425.

(6) Reedijk, J. *Proc. Natl. Acad. Sci. U.S.A.* **2003**, *100*, 3611−3616.

(7) Sherman, S. E.; Gibson, D.; Wang, A. H.; Lippard, S. J. *Science* **1985**, *230*, 412−417.

(8) Comess, K. M.; Lippard, S. J. In *Molecular Aspects of Anticancer Drug−DNA Interactions*; Neidle, S., Waring, M., Eds.; Macmillan Press: London, 1993; pp 134−168.

(9) Lippert, B. *Cisplatin: Chemistry and Biochemistry of a leading anticancer drug*, 1st ed.; Wiley-VCH: Weinheim, Germany, 1999.

(10) Eichhorn, G. L.; Marzilli, L. G. *Metal Ions in Genetic Information Transfer*; Elsevier: New York, 1981.

(11) Sigel, H.; Sigel, A. *Interactions of Metal Ions with Nucleotides, Nucleic Acids and Their Constituents.* Dekker M.: New York, 1996; Ref Type: Serial (Book, Monograph), 32.

(12) Legendre, F.; Kozelka, J.; Chottard, J. C. *Inorg. Chem.* **1998**, *37*, 3964−3967.

(13) Lippert B. *Prog. Inorg. Chem.* **1989**, *37*, 1−9.

(14) Reedijk, J. *Chem. Rev.* **1999**, *99*, 2499−2510.

(15) Comess, K. M.; Burstyn, J. N.; Essigmann, J. M.; Lippard, S. J. *Biochemistry* **1992**, *31*, 3975−3990.

(16) Jamieson, E. R.; Lippard, S. J. *Chem. Rev.* **1999**, *99*, 2467−2498.

(17) Kasparkova, J.; Delalande, O.; Stros, M.; Elizondo-Riojas, M. A.; Vojtiskova, M.; Kozelka, J.; Brabec, V. *Biochemistry* **2003**, *42*, 1234−1244.

(18) Takahara, P. M.; Frederick, C. A.; Lippard, S. J. *J. Am. Chem. Soc.* **1996**, *118*, 12309−12321.

(19) Marzilli L. G.; Saad J. S.; Kuklenyik Z.; Keating K. A.; Xu Y. *J. Am. Chem. Soc.* **2001**, *123*, 2764−2770.

(20) Yang D.; van Boom, S. S. G. E.; Reedijk, J.; van Boom, J. H.; Wang, A. H.-J. *Biochemistry* **1995**, *34*, 12912−12920.
(21) Fichtinger-Schepman, A. M.; van der Veer, J. L.; den Hartog, J. H.; Lohman, P. H.; Reedijk, J. *Biochemistry* **1985**, *24*, 707−713.
(22) Jung, Y.; Lippard, S. J. *Biochemistry* **2003**, *42*, 2664−2671.
(23) Yoshioka, K.; Saito, K.; Tanabe, T.; Yamamoto, A.; Ando, Y.; Nakamura, Y.; Shirakawa, H.; Yoshida, M. *Biochemistry* **1999**, *38*, 589−595.
(24) He, Q.; Ohndorf, U. M.; Lippard, S. J. *Biochemistry* **2000**, *39*, 14426−14435.
(25) Cohen, S. M.; Mikata Y.; He Q.; Lippard, S. J. *Biochemistry* **2000**, *39*, 11771−11776.
(26) Pasheva, E. A.; Ugrinova, I.; Spassovska, N. C.; Pashev, I. G. *Int. J. Biochem. Cell Biol.* **2002**, *34*, 87−92.
(27) Chu, G. *J. Biol. Chem.* **1994**, *269*, 787−790.
(28) Fuertes, M. A.; Alonso, C.; Perez, J. M. *Chem. Rev.* **2003**, *103*, 645−662.
(29) Gonzalez, V. M.; Fuertes, M. A.; Alonso, C.; Perez, J. M. *Mol. Pharmacol.* **2001**, *59*, 657−663.
(30) Fuertes, M. A.; Castilla, J.; Alonso, C.; Perez, J. M *Curr. Med. Chem. Anti-Canc. Agents* **2002**, *2*, 539−551.
(31) Bose, R. N. *Mini Rev. Med. Chem.* **2002**, *2*, 103−111.
(32) van Boom, S. S. G. E.; Yang, D.; Reedijk, J.; van der Marel, G. A.; Wang, A. H.-J. *J. Biomol. Struct. Dyn.* **1996**, *13*, 989−998.
(33) Ohndorf, U. M.; Whitehead, J. P.; Raju, N. L.; Lippard, S. J. *Biochemistry* **1997**, *36*, 14807−14815.
(34) Teuben, J. M.; Bauer, C.; Wang, A. H.; Reedijk, J. *Biochemistry* **1999**, *38*, 12305−12312.
(35) Blackburn, G. M.; Gait, M. J. *Nucleic Acids in Chemistry and Biology*.; Oxford Universtiy Press: Oxford, U.K., 1996.
(36) Pelmenschikov, A.; Zilberberg, I.; Leszczynski, J.; Famulari, A.; Sironi, M.; Raimondi, M. *Chem. Phys. Lett.* **1999**, *314*, 496−500.
(37) Parkinson, J. A.; Chen, Y.; Murdoch, P.d. S.; Guo, Z.; Berners-Price, S. J.; Brown, T.; Sadler, P. J. *Chem.-Eur. J.* **2000**, *6*, 3636−3644.
(38) Herman, F.; Kozelka, J.; Stoven, V.; Guittet, E.; Girault, J. P.; Huynh-Dinh, T.; Igolen, J.; Lallemand, J. Y.; Chottard, J. C. *Eur. J. Biochem.* **1990**, *194*, 119−133.
(39) Kozelka, J. *Met. Ions. Biol. Syst.* **1996**, *33*, 1−28.
(40) Yao, S.; Plastaras, J. P.; Marzilli, L. G. *Inorg. Chem.* **1994**, *33*, 6061−6077.
(41) Elizondo-Riojas, M. A.; Kozelka, J. *J. Mol. Biol.* **2001**, *314*, 1227−1243.
(42) Banci, L. C. P. *Molecular Modeling and dynamics of bioinorganic compounds*; Kluwer Academic Publishers: Dordrecht, The Netherlands, 1997.
(43) Elizondo-Riojas, M. A.; Gonnet, F.; Auge-Barrere-Mazouat, P.; Allain, F.; Berges, J.; Attias, R.; Chottard, J.-C.; Kozelka, J. Molecular Modeling of Platinum Complexes with Oligonucleotides: Methodological Lessons and Structural Insights. In *Molecular Modeling and dynamics of bioinorganic compounds*; Banci, L. C. P., Ed.; Kluwer Academic Publishers: Dordrecht, The Netherlands, 1997; pp 131−160.
(44) Brabec, V.; Sip, M.; Leng, M. *Biochemistry* **1993**, *32*, 11676−11681.
(45) Sip, M.; Schwartz, A.; Vovelle, F.; Ptak, M.; Leng, M. *Biochemistry* **1992**, *31*, 2508−2513.
(46) Burda, J. V.; Sponer, J.; Leszczynski, J. *Phys. Chem. Chem. Phys.* **2001**, *3*, 4404−4411.
(47) Burda, J. V.; Sponer, J.; Leszczynski, J. *J. Biol. Inorg. Chem.* **2000**, ***5***, 178−188.
(48) Cohen, G. L.; Bauer, W. R.; Barton, J. K.; Lippard, S. J. *Science* **1979**, *203*, 1014−1016.
(49) Carloni, P.; Sprik, M.; Andreoni, W. *J. Phys. Chem. B* **2000**, *104*, 823−835.
(50) Laio, A.; VandeVondele, J.; Rothlisberger, U. *J. Phys. Chem. B* **2002**, *106*, 7300−7307.
(51) Laio, A.; VandeVondele, J.; Rothlisberger, U. *J. Chem. Phys.* **2002**, *116*, 6941.
(52) Hutter, J.; Alavi, A.; Deutsch, T.; Silvestri, W.; Parrinello, M.; Rothlisberger, U.; Marx, D.; Focher, P.; Tuckerman, M.; Andreoni, W.; Curioni, A.; Fois, E.; Giannozzi, P.; Sebastiani, D.; Laio, A.; VandeVondele, J.; Seitsonen, A.; Billeter, S. CPMD.MPI fuer Festkoerperforschung Stuttgard and IBM Zurich Research Laboratory (3.4.), 2000.
(53) Carloni, P.; Andreoni, W. *J. Chem. Phys.* **1996**, *100*, 17797−17800.
(54) Bouten, R.; Baerends, E. J.; van Lenthe, E.; Visscher, L.; Schreckenbach, G.; Ziegler, T. *J. Phys. Chem. A* **2000**, *104*, 5600−5611.
(55) Schreckenbach, G.; Wolff, S. K.; Ziegler, T. *J. Phys. Chem. A* **2000**, *104*, 8244−8255.
(56) Case, D. A.; Pearlman, D. A.; Caldwell, J. W.; Cheatham, T. E., III.; Ross, W. S.; Simmerling, C. L.; Darden, T. A.; Merz, K. M.; Stanton, R. V.; Cheng, A. L.; Vincent, J. J.; Crowley, M.; Tsui, V.; Radner, R. J.; Duan, Y.; Pitera, J.; Massova, I.; Seibel, G. L.; Singh, U. C.; Weiner, P. K.; Kollman, P. A. AMBER6. University of California: San Francisco, CA, 1999.
(57) Pearlman, D. A.; Case, D. A.; Caldwell, J. W.; Ross, W. S.; Cheatham, T. E., III; DeBolt, S.; Ferguson, D.; Seibel, G. L.; Kollman, P. A. *Comput. Phys. Commun.* **1995**, *91*, 1−41.
(58) Cornell, W. D.; Cieplak, P.; Bayly, C. I.; Gould, I. R.; Merz, K. M., Jr.; Ferguson, D. M.; Spellmeyer, D. C.; Fox, T.; Caldwell, J. W.; Kollman, P. A. *J. Chem. Phys.* **1995**, *117*, 5179−5197.
(59) Cheatham, T. E., III.; Cieplak, P.; Kollman, P. A. *J. Biomol. Struct. Dyn.* **1999**, *16*, 845−862.
(60) Joergens, W. L. *J. Chem. Phys.* **1983**, *79*, 926−935.
(61) Cheatham, T. E., III.; Miller, J. L.; Fox, T.; Darden, T. A.; Kollman, P A. Molecular dynamics simulations on solvated biomolecular systems: the Particle Mesh Ewald method leads to stable trajectories of DNA, RNA, and proteins. *J. Am. Chem. Soc.* **1995**, *117*, 4193−4194.
(62) Berendsen, H. J. C.; Postma, J. P. M.; van Gunsteren, W. F.; DiNola, A.; Haak, J. R. *J. Chem. Phys.* **1984**, *81*, 3684−3690.
(63) van Gunsteren, W. F. *Biomolecular Simulation: The GROMOS96 Manual and User Guide*; Hochschulverlag AG der ETH Zuerich: Zuerich, Groningen, 1996.
(64) Sebastiani, D.; Rothlisberger, U. Advances in Density-functional-based Modeling Techniques- Recent Extensions of the Car-Parrinello Approach. In *Quantum Medicinal Chemistry*; Carloni, P., Alber, F., Eds.; Wiley-VCH: Weinheim, Germany, 2003; pp 5−36.
(65) Rothlisberger, U.; Carloni, P. Simulations of enzymatic systems: Perspectives from Car-Parrinello Molecular dynamics simulations. Eriksson L. A. *Theoretical and computational chemistry*; Politzer, P.; Maksic, Z. B., Eds.; Elsevier: Amsterdam, 2001; Vol. 9, pp 215−251.
(66) Troullier, N.; Martins, J. L. *Phys. Rev. B* **1991**, *43*, 1943−2006.
(67) Kleinman, L.; Bylander, D. M. *Phys. Rev. Lett.* **1982**, *48*, 1425.
(68) Becke, A. D. *Phys. Rev. A* **1988**, *38*, 3098−3100.
(69) Lee, C.; Yang, W.; Parr, R. G. *Phys. Rev. B* **1988**, *37*, 785−789.
(70) Barnett, R. N.; Landman, U. *Phys. Rev. B* **1993**, *48*, 2081−2097.
(71) Nose, S. J. *J. Chem. Phys.* **1984**, *81*, 511−519.
(72) Hoover, W. G. *Phys. Rev. A* **1985**, *31*, 1695−1697.
(73) Dickerson, R. E. *J. Biomol. Struct. Dyn.* **1989**, *6*, 627−634.
(74) Swaminathan, S.; Ravishanker, G.; Beveridge, D. L.; Lavery, R.; Etchebest, C.; Sklenar, H. *Proteins* **1990**, *8*, 179−193.
(75) Lavery, R.; Sklenar, H. *J. Biomol. Struct. Dyn.* **1989**, *6*, 655−667.
(76) te Velde, G.; Snijders, G. J.; Ziegler, T.; van Gisbergen, S. J. A.; Fonseca Guerra, C.; Baerends, E. J.; Bickelhaupt, F. M. *J. Comput. Chem.* **2001**, *22*, 931−967.
(77) Fonseca Guerra, C.; Snijdeers, J. G.; te Velde, G.; Baerends, E.-J. Parallelisation of the Amsterdam Density Functional Program. In *Methods and Techniques for Computational Chemistry*; Clementi, E., Corongiu, C., Eds.; STEF: Cagliari, 1995; pp 303−395.
(78) Baerends, E.-J.; Autschbach, J.; Berces, A.; Bo, C.; Boerrigter, P. M.; Cavallo, L.; Chong, D. P.; Deng, L.; Dickson, R. M.; Ellis, D. E.; Fan, L.; Fischer, T. H.; Fonseca Guerra, C.; van Gisbergen, S. J. A. *ADF2002.3*, *SCM, Theoretical Chemistry*, (2002.03); Vrije Universiteit: Amsterdam, The Netherlands, 2002.
(79) Perdew, J. P. *Phys. Rev. Lett.* **1985**, *55*, 1665−1668.
(80) Perdew, J. P. *Phys. Rev. B* **1986**, *33*, 8822−8824.
(81) Schreckenbach, G. *Inorg. Chem.* **2002**, *41*, 6560−6572.
(82) Wolff, S. K.; Ziegler, T.; van Lenthe, E.; Baerends, E.-J. *J. Chem. Phys.* **1999**, *110*, 7689−7698.
(83) Gilbert, T. M.; Ziegler, T. *J. Phys. Chem. A* **1999**, *103*, 7535−7543.
(84) van Lenthe, E.; Ehlers, A.; Baerends, E.-J. *J. Chem. Phys.* **1999**, *110*, 8943−8953.
(85) Cheatham, T. E., III.; Kollman, P. A. *J. Mol. Biol.* **1996**, *259*, 434−444.
(86) Brugé, F.; Bernasconi, M.; Parrinello, M. *J. Am. Chem. Soc.* **1999**, *121*, 10883−10888.
(87) Schmidt, K. S.; Boudvillain, M.; Schwartz, A.; van der Marel, G. A.; van Boom, J. H.; Reedijk, J.; Lippert, B. *Chemistry*. **2002**, *8*, 5566−5570.
(88) Kasparkova, J.; Marini, V.; Najajreh, Y.; Gibson, D.; Brabec, V. *Biochemistry* **2003**, *42*, 6321−6332.
(89) Bloemink, M. J.; Reedijk, J. *Met. Ions. Biol. Syst.* **1996**, *32*, 641−685.
(90) Jansen, B. A.; van der Zwan, J.; den Dulk, H.; Brouwer, J.; Reedijk, J. *J. Med. Chem.* **2001**, *44*, 245−249.
(91) Janik, M. B.; Lippert, B. *J. Biol. Inorg. Chem.* **1999**, *4*, 645−653.
(92) Coste, F.; Malinge, J. M.; Serre, L.; Shepard, W.; Roth, M.; Leng, M.; Zelwer, C. *Nucleic Acids Res.* **1999**, *27*, 1837.
(93) Huang, H.; Zhu, L.; Reid, B. R.; Drobny, P.; Hopkins, P. B. *Science* **1995**, *270*, 1842.
(94) Coste, F.; Shepard, W.; Zelwer, C. *Acta Crystallogr., Sect. D* **2002**, *58*, 431.
(95) Wing, R. M.; Pjura, P.; Drew, H. R.; Dickerson, R. E. *EMBO J.* **1984**, *3*, 1201.